unique ligand and the solvent DMF. Subsequent iterations of least squares cycles and difference Fourier calculations revealed solvent disorder. The solvent disorder was successfully modeled with 0.57/0.43 occupancies for all except the O4 of the solvent DMF. In the latter cycles of refinement, hydrogen atoms were included at calculated positions for structure factor calculations but were not refined. Full matrix least-squares refinement yielded $R = 0.051$ and $R_w = 0.058$ for 199 parameters and 1247 reflections with $I \geq 3\sigma(I)$. Positional parameters are listed in Table V.[42]

Acknowledgment. This research was funded by the National Institutes of Health Grant AI 11744. The authors also wish to acknowledge Mr. Ryan Powers for performing the MM2 calculations on the Δ and Λ vanadium complexes of the linear trimer and enterobactin.

Supplementary Material Available: Tables of bond lengths, bond angles, torsional angles, anisotropic thermal parameters, and positional parameters for the two structures $K_2[V(ent)]\cdot 3DMF$ and $K_2[V(eba)_3]\cdot 3DMF$, ORTEP views of the potassium coordination in both structures, and the UV/vis spectrum of the complex $[V(eba)_3]^{2-}$ (18 pages). Ordering information is given on any current masthead page.

Dioxygen Binding to Diferrous Centers. Models for Diiron–Oxo Proteins†

Yanhong Dong, Stéphane Ménage, Bridget A. Brennan, Timothy E. Elgren, Ho G. Jang, Linda L. Pearce, and Lawrence Que, Jr.*

Contribution from the Department of Chemistry, University of Minnesota, Minneapolis, Minnesota 55455. *Received August 24, 1992*

Abstract: Dioxygen adducts of $[Fe_2L(O_2CC_6H_5)]X_2$, where L represents the dinucleating ligands HPTB (anion of *N,N,N′,N′*-tetrakis(2-benzimidazolylmethyl)-2-hydroxy-1,3-diaminopropane), its *N*-ethyl analogue, and its tetrakis(pyridine) analogue, HPTP, can form and serve as models for the putative oxygenated intermediates of methane monooxygenase and ribonucleotide reductase. $[Fe_2(N\text{-Et-HPTB})(O_2CC_6H_5)](BF_4)_2$ (**1**) crystallizes in the triclinic space group $P\bar{1}$ with cell constants $a = 13.04$ (1) Å, $b = 14.248$ (7) Å, $c = 18.09$ (1) Å, $\alpha = 73.56$ (6)°, $\beta = 78.22$ (7)°, $\gamma = 67.71$ (6)°, $V = 2963$ (9) Å^3, $Z = 2$; $R = 0.069$, and $R_w = 0.085$. The Fe(II) sites are bridged by the alkoxide of the dinucleating ligand and a benzoate, affording a diiron core with an Fe–μ–O–Fe angle of 124.0 (3)° and an Fe–Fe distance of 3.473 (7) Å. Both Fe(II) centers have trigonal bypyramidal geometry, and NMR studies show that the remaining coordination sites are accessible to ligands such as DMSO and Ph_3PO. The iron centers are antiferromagnetically coupled with $J \sim 20$–26 cm^{-1} ($\mathcal{H} = JS_1\cdot S_2$). Irreversible dioxygen adducts form upon exposure of the diferrous complexes to O_2 at low temperatures. The $\mathbf{1}/O_2$ adduct and its HPTB analogue, $\mathbf{2}/O_2$, are stable indefinitely in CH_2Cl_2 at −60 °C but decompose upon warming; the addition of DMSO or other polar aprotic solvents further stabilizes the adducts, allowing them to persist for short periods even at ambient temperature. The adduct of the pyridine analogue, $\mathbf{3}/O_2$, on the other hand, is not observed at −80 °C unless a polar aprotic solvent is added to the CH_2Cl_2 solution. The adducts exhibit visible absorption maxima near 600 nm and resonance Raman features at ∼470 cm^{-1} (ν(Fe–O)) and ∼890–900 cm^{-1} (ν(O–O)). The latter is characteristic of a μ-1,2-peroxo species; in support, the NMR properties of the HPTB adducts indicate the presence of a moderately strong antiferromagnetic coupling interaction ($J \sim 140$ cm^{-1}). Carboxylate substitution on **1** effects a shift of the absorption maximum of the adduct, indicating that the carboxylate remains coordinated in the adduct. Thus, the adducts are proposed to have tribridged (μ-1,2-peroxo)(μ-carboxylato)(μ-alkoxo)diferric cores. The differing stabilities of the dioxygen adducts are also reflected in differences in reactivity. The addition of 2,4-di-*tert*-butylphenol or Ph_3P does not affect the $\mathbf{1}/O_2$ adduct at −50 °C but does accelerate the decomposition of the $\mathbf{3}/O_2$ adduct, affording 0.5–0.6 equiv of the corresponding biphenol or $OPPh_3$, respectively. The one-electron oxidation of a phenol by $\mathbf{3}/O_2$ suggests that such an oxygenated species may be involved in the mechanism of the tyrosyl radical formation in ribonucleotide reductase; however, some further activation step is likely to be required for such a species to participate in the alkane hydroxylation mechanism of methane monooxygenase.

Introduction

Diiron centers that are known to interact with dioxygen[1] have been found in hemerythrin (Hr),[2,3] ribonucleotide reductase (RNR),[4–7] and methane monooxygenase (MMO).[8,9] DeoxyHr reversibly binds dioxygen to form oxyHr, characterized as a (μ-oxo)diiron(III) complex with a terminally bound hydroperoxide.[3] The adduct exhibits a purple color ($\lambda_{max} = 500$ nm) ascribed to a peroxide-to-iron(III) charge-transfer band.[10] The diferrous form of the R2 protein of ribonucleotide reductase also reacts with dioxygen to form a colored intermediate ($\lambda_{max} = 565$ nm) proposed to be a dioxygen adduct of the diiron active site which decays to the active protein containing the catalytically essential tyrosine radical.[11] The diferrous form of the hydroxylase of methane monooxygenase (MMO) has been demonstrated to react with dioxygen,[9a] but no intermediate has been observed; additionally, its diferric form reacts with H_2O_2 to oxidize alkanes in a peroxide shunt mechanism analogous to that observed for cytochrome

† Dedicated to Professor Richard H. Holm in celebration of his 60th birthday.

(1) Que, L., Jr.; True, A. E. *Prog. Inorg. Chem.* **1990**, *38*, 97–200.
(2) (a) Wilkins, P. C.; Wilkins, R. G. *Coord. Chem. Rev.* **1987**, *79*, 195–214. (b) Klotz, I. M.; Kurtz, D. M., Jr. *Acc. Chem. Res.* **1984**, *17*, 16–22.
(3) (a) Holmes, M. A.; Trong, I. L.; Turley, S.; Sieker, L. C.; Stenkamp, R. E. *J. Mol. Biol.* **1991**, *218*, 583–593. (b) Sheriff, S.; Hendrickson, W. A.; Smith, J. L. *J. Mol. Biol.* **1987**, *197*, 273–296. (c) Stenkamp, R. E.; Sieker, L. C.; Jensen, L. H.; McCallum, J. D.; Sanders-Loehr, J. *Proc. Natl. Acad. Sci. U.S.A.* **1985**, *82*, 713–716.
(4) Reichard, P.; Ehrenberg, A. *Science (Washington, D.C.)* **1983**, *221*, 514–519.
(5) Nordlund, P.; Sjöberg, B.-M.; Eklund, H. *Nature* **1990**, *345*, 593–598.
(6) Lynch, J. B.; Juarez-Garcia, C.; Münck, E.; Que, L., Jr. *J. Biol. Chem.* **1989**, *264*, 8091–8096.
(7) Sahlin, M.; Gräslund, A.; Petersson, L.; Ehrenberg, A.; Sjöberg, B.-M. *Biochemistry* **1989**, *28*, 2618–2625.
(8) DeWitt, J. G.; Bentsen, J. G.; Rosenzweig, A. C.; Hedman, B.; Green, J.; Pilkington, S.; Papaefthymiou, G. C.; Dalton, H.; Hodgson, K. O.; Lippard, S. J. *J. Am. Chem. Soc.* **1991**, *113*, 9219–9235.

0002-7863/93/1515-1851$04.00/0

P-450.[12] Radical-free diferric ribonucleotide reductase also reacts with H_2O_2 to generate the tyrosine radical.[13]

Synthetic efforts in this area have recently focused on modeling the diferrous active sites of these proteins. Wieghardt et al.[14] reported the synthesis and structure of $[Fe_2(OH)(OAc)_2(Me_3TACN)_2]X$,[15] which models the antiferromagnetically coupled (μ-hydroxo)bis(μ-carboxylato) core found for deoxyHr. Borovik et al.[16] characterized $[Fe_2(O_2CR)_2BPMP]X$ complexes with (μ-phenoxo)bis(μ-carboxylato) cores which exhibit the low-field $g \sim 16$ integer spin EPR signals found for a number of the diiron–oxo proteins in their diferrous oxidation states.[6,9,17] Tolman et al.[18] synthesized the complex $[Fe_2(BIPhMe)_2(O_2CH)_4]$ with a (μ-formato-*O*)bis(μ-formato-*O*,*O*') core that mimics the unsymmetric diiron coordination environment found in deoxyHr; one Fe(II) ion is 6-coordinate, while the other is pseudo-5-coordinate with the carbonyl oxygen of the monodentate formate bridge acting as a weak sixth ligand. Mênage et al.[19] obtained $[Fe_2(TPA)_2(OAc)_2](BPh_4)_2$ with a bis(μ-carboxylato-*O*,*O*') core that models the putative diiron site of reduced RNR R2.[20] Exposure of these diferrous complexes to dioxygen results in their oxidation, but no dioxygen adducts have been observed in the course of the reactions.

Dioxygen binding has been observed for several ferrous precursors, all of which have available coordination sites for O_2. Kitajima et al. reported the structure of the 6-coordinate [Fe{HB(3,5-*i*-Pr_2pz)$_3$}(OBz)(CH_3CN)], which reversibly binds O_2 presumably by displacing the coordinated solvent.[21] The O_2 adduct is proposed to have a (μ-1,2-peroxo)diiron(III) unit on the basis of spectroscopic data. Similarly, we found that $[Fe^{II}_2(N\text{-Et-HPTB})OBz](BF_4)_2$,[22] a complex with two 5-coordinate iron centers, irreversibly binds O_2 to form a (μ-1,2-peroxo)diiron(III) adduct. Using a related dinucleating ligand with sterically encumbering 6-methylpyridyl groups in place of the *N*-ethylbenzimidazolyl groups, Suzuki et al. prepared $[Fe^{II}_2(6\text{-Me-HPTP})OBz(H_2O)](BF_4)_2$, the O_2 adduct of which is reversible.[23] None of these adducts has thus far been crystallized. Indeed, the only crystallographically characterized nonheme-iron dioxygen complex is $[Fe_6(O)_2(O_2)(O_2CPh)_{12}(OH_2)_2]$,[24] which is derived from the addition of H_2O_2 to a hexaferric precursor and has a (μ_4-peroxo)tetrairon unit.

In this paper, we report details of the crystal structure of the diferrous precursor $[Fe^{II}_2(N\text{-Et-HPTB})OBz](BF_4)_2$ (**1**), its properties and those of the analogous HPTB (**2**) and HPTP (**3**) complexes, and the spectroscopic and reactivity properties of their dioxygen adducts.

Table I. Details of the Crystallographic Experiments and Computations[a] for **1**

formula	$C_{56}H_{63}B_2F_8Fe_2N_{13}O_3$
fw	1251.52
temp, K	159
cryst syst	triclinic
space group	$P\bar{1}$ (No. 2)
a, Å	13.04 (1)
b, Å	14.248 (7)
c, Å	18.09 (1)
α, deg	73.56 (6)
β, deg	78.22 (7)
γ, deg	67.61 (6)
V, Å^3	2963 (9)
Z	2
ρ(calc), g cm^{-3}	1.247
radiation	Mo Kα (λ = 0.7107 Å)
$\mu_{Mo K\alpha}$, cm^{-1}	5.56
scan type	ω–2θ
$2\theta_{max}$, deg	49.9
no. of reflns	9357
no. of unique data with $I > 3\sigma(I)$	4733
no. of variables	734
R^b	0.069
$R_w{}^b$	0.085

[a] The intensity data were processed as described in: *CAD 4 and SDP-PLUS User's Manual*; B. A. Frenz & Associates: College Station, TX, 1982. The net intensity $I = [K(\text{NPI})](C - 2B)$, where K = 20.1166 (attenuator factor), NPI = ratio of fastest possible scan rate to scan rate for the measurement, C = total count, and B = total background count. The standard deviation in the net intensity is given by $[\sigma(I)]^2 = (k/\text{NPI})^2[C + 4B + (pI)^2]$, where p is a factor used to downweigh intense reflections. The observed structure factor amplitude F_o is given by $F_o = (I/Lp)^{1/2}$, where Lp = Lorentz–polarization factor. The $\sigma(I)$'s were converted to the estimated errors in the relative structure factors $\sigma(F_o)$ by $\sigma(F_o) = {}^1/_2[\sigma(I)/I]F_o$. [b] $R = (\sum||F_o| - |F_c||)/(\sum F_o)$; $R_w = [(\sum w|F_o - F_c|^2)/(\sum w(F_o)^2)]^{1/2}$.

Experimental Section

Synthesis. The dinucleating ligands HPTB and *N*-Et-HPTB were synthesized using the published procedures.[25,26] HPTP was synthesized by the reaction of epichlorohydrin with bis(2-pyridylmethyl)amine.[27] A 14.7% aqueous solution of bis(2-pyridylmethyl)amine (3.06 g, 15.4 mmol) was adjusted to about pH 8 by adding 6 N HCl. The solution was maintained at about 70–75 °C and pH 8 while 0.71 g (7.7 mmol) epichlorohydrin was added slowly to the solution. After 4 h, the solution was then cooled to about 0 °C, and 70% $HClO_4$ was added to the solution until no more yellow precipitate formed. After filtration, the yellow precipitate was washed with cold MeOH and dried in vacuo. ^{1}H NMR and mass spectrometry indicated that the yellow solid was HPTP·4$HClO_4$ (3.51 g; yield, 53.4%). ^{1}H NMR (D_2O), δ (ppm): 2.7 (m, 4H), 4.3 (m, 9H), 7.9 (m, 8H), 8.5 (t, 4H), 8.7 (d, 4H). Mass spectrometry (negative-ion FAB): *m/z* 855.2. *Caution*: The perchlorate salt in this study is potentially explosive and should be handled with care.

$[Fe^{II}_2(N\text{-Et-HPTB})(OBz)](BF_4)_2$ (**1**) was prepared under argon by dissolving HOBz (0.06 g, 0.5 mmol), Et_3N (70 μL, 1.0 mmol), and H-*N*-Et-HPTB (0.36 g, 0.5 mmol) in 20 mL of MeOH and transferring

(9) (a) Fox, B. G.; Froland, W. A.; Dege, J. E.; Lipscomb, J. D. *J. Biol. Chem.* **1989**, *264*, 10023–10033. (b) Fox, B. G.; Surerus, K. K.; Münck, E.; Lipscomb, J. D. *J. Biol. Chem.* **1988**, *263*, 10553–10556.
(10) Shiemke, A. K.; Loehr, T. M.; Sanders-Loehr, J. *J. Am. Chem. Soc.* **1984**, *106*, 4951–4956.
(11) Bollinger, J. M., Jr.; Edmondson, D. E.; Huynh, B. H.; Filley, J.; Norton, J. R.; Stubbe, J. *Science (Washington, D.C.)* **1991**, *253*, 292–298.
(12) Andersson, K. K.; Froland, W. A.; Lee, S.-K.; Lipscomb, J. D. *New J. Chem.* **1991**, *15*, 411–415.
(13) (a) Fontecave, M.; Gerez, C.; Atta, M.; Jeunet, A. *Biochem. Biophys. Res. Commun.* **1990**, *168*, 659–664. (b) Sahlin, M.; Sjöberg, B.-M.; Backes, G.; Loehr, T.; Sanders-Loehr, J. *Biochem. Biophys. Res. Commun.* **1990**, *167*, 813–818.
(14) (a) Chaudhuri, P.; Wieghardt, K.; Nuber, B.; Weiss, J. *Angew. Chem., Int. Ed. Engl.* **1985**, *24*, 778–779. (b) Hartman, J. R.; Rardin, R. L.; Chaudhuri, P.; Wieghardt, K.; Nuber, B.; Weiss, J.; Papaefthymiou, G. C.; Frankel, R. B.; Lippard, S. J. *J. Am. Chem. Soc.* **1987**, *109*, 7387–7395.
(15) Abbreviations used: BIPhMe = bis(1-methyl-2-imidazolyl)phenylmethoxymethane; BPMP = 2,6-bis(bis((2-pyridylmethyl)amino)methyl)-4-methylphenol; H_4EDTA = *N*,*N*'-ethylenebis(*N*-(carboxymethyl)glycine); HPTB = *N*,*N*,*N*',*N*'-tetrakis(2-benzimidazolylmethyl)-2-hydroxy-1,3-diaminopropane; HPTP = *N*,*N*,*N*',*N*'-tetrakis(2-pyridylmethyl)-1,3-diamino-2-hydroxypropane; L = HB(3,5-*i*-Pr_2pz)$_3$; 5-Me-HXTA = *N*,*N*'-(2-hydroxy-5-methyl-1,3-xylylene)bis(*N*-(carboxymethyl)glycine); Me_3TACN = 1,4,7-trimethyl-1,4,7-triazacyclononane; NTB = tris((2-benzimidazolyl)methyl)-amine; OEP = octaethylporphyrin; OBz = benzoate; pz = pyrazole; TPA = tris(2-pyridylmethyl)amine.
(16) (a) Borovik, A. S.; Que, L., Jr. *J. Am. Chem. Soc.* **1988**, *110*, 2345–2346. (b) Borovik, A. S.; Hendrich, M. P.; Holman, T. R.; Münck, E.; Papaefthymiou, V.; Que, L., Jr. *J. Am. Chem. Soc.* **1990**, *112*, 6031–6038.
(17) (a) Reem, R. C.; Solomon, E. I. *J. Am. Chem. Soc.* **1987**, *109*, 1216–1226. (b) Hendrich, M. P.; Pearce, L. L.; Que, L., Jr.; Chasteen, N. D.; Day, E. P. *J. Am. Chem. Soc.* **1991**, *113*, 3039–3044.
(18) (a) Tolman, W. B.; Bino, A.; Lippard, S. J. *J. Am. Chem. Soc.* **1989**, *111*, 8522–8523. (b) Tolman, W. B.; Liu, S.; Bentsen, J. G.; Lippard, S. J. *J. Am. Chem. Soc.* **1991**, *113*, 152–164.
(19) Mênage, S.; Zang, Y.; Hendrich, M. P.; Que, L., Jr. *J. Am. Chem. Soc.* **1992**, *114*, 7786–7792.
(20) Atta, M.; Nordlund, P.; Åberg, A.; Eklund, H.; Fontecave, M. *J. Biol. Chem.* **1992**, *267*, 20682–20688.
(21) Kitajima, N.; Hideno, F.; Moro-oka, Y.; Mizutani, Y.; Kitagawa, T. *J. Am. Chem. Soc.* **1990**, *112*, 6402–6403.
(22) Mênage, S.; Brennan, B. A.; Juarez-Garcia, C.; Münck, E.; Que, L., Jr. *J. Am. Chem. Soc.* **1990**, *112*, 6423–6425.
(23) Hayashi, Y.; Suzuki, M.; Uehara, A.; Mizutani, Y.; Kitagawa, T. *Chem. Lett.* **1992**, 91–94.
(24) Micklitz, W.; Bott, S. G.; Bentsen, J. G.; Lippard, S. J. *J. Am. Chem. Soc.* **1989**, *111*, 372–374.
(25) McKee, V.; Zvagulis, M.; Dagdigian, J. V.; Patch, M. G.; Reed, C. A. *J. Am. Chem. Soc.* **1984**, *106*, 4765–4772.
(26) Chen, Q.; Lynch, J. B.; Gomez-Romero, P.; Ben-Hussein, A.; Jameson, G. B.; O'Connor, C. J.; Que, L., Jr. *Inorg. Chem.* **1988**, *27*, 2673–2681.
(27) Scanlon, P. M.; Thunberg, J. C. U.S. Patent 3,780,100, 1973.

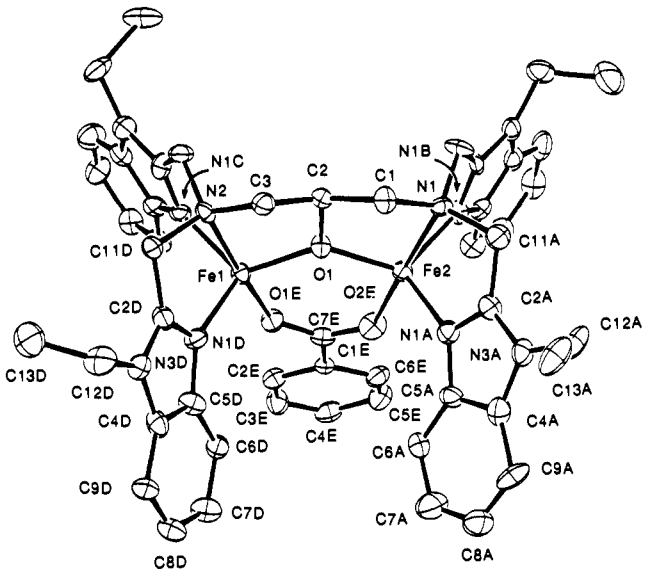

Figure 1. ORTEP plot of the $[Fe_2(N\text{-Et-HPTB})OBz]^{2+}$ cation showing 50% probability ellipsoids. Atom labels for benzimidazoles B and C as well as all hydrogen atoms have been omitted for clarity; the numbering schemes for rings B and C are analogous to those for rings A and D.

the solution anaerobically to solid $Fe(BF_4)_2{\cdot}6H_2O$ (0.34 g, 1.0 mmol). Clear yellow crystals of **1** of crystallographic quality were obtained after 2 days in a glovebox by slow diffusion of Et_2O into a CH_3CN solution. Anal. Calcd for $C_{50}H_{54}B_2F_8Fe_2N_{10}O_3$: C, 53.24; H, 4.78; N, 12.40. Found: C, 53.30; H, 4.86; N, 12.09. The analogous $[Fe^{II}_2(N\text{-Et-HPTB})(O_2CC_2H_5)](BF_4)_2$ and $[Fe^{II}_2(HPTB)(OBz)](BF_4)_2$ (**2**) complexes were synthesized following the same procedure.

$[Fe^{II}_2(HPTP)(OBz)](BPh_4)_2$ (**3**) was prepared under argon by dissolving HPTP·$4HClO_4$ (0.214 g, 0.25 mmol), HOBz (0.0305 g, 0.25 mmol), and Et_3N (0.139 g, 1.37 mmol) in 10 mL of MeOH and transferring the solution anaerobically to solid $Fe(BF_4)_2{\cdot}6H_2O$ (0.169 g, 0.50 mmol). The addition of a degassed methanol solution of $NaBPh_4$ (0.171 g, 0.50 mmol, 10 mL) yielded a yellow precipitate which was filtered off, dried in vacuo, and recrystallized from acetonitrile/ether. Anal. Calcd for $C_{82}H_{74}B_2Fe_2N_6O_3$: C, 74.34; H, 5.63; N, 6.34. Found: C, 74.31; H, 5.69; N, 6.44.

The dioxygen adducts of the diferrous complexes were prepared by chilling the appropriate anaerobic precursor solution to −60 or −80 °C and bubbling O_2 through the solution. $^{18}O_2$ (97% isotopic abundance) used in the Raman experiments was purchased from Isotec.

Crystallographic Results for $[Fe^{II}_2(N\text{-Et-HPTB})(OBz)](BF_4)_2$. X-ray diffraction data were collected on a crystal of $[Fe^{II}_2(N\text{-Et-HPTB})(OBz)](BF_4)_2$ by an Enraf-Nonius CAD4 diffractometer in the University of Minnesota Crystallography Facility. Crystal data, together with details of the diffraction experiment and subsequent calculations, are listed in Table I. The cell dimensions were obtained by least-squares refinement of the setting angles for 25 reflections (2θ = 16.00–30.60°). The stability of the crystal was monitored during data collection by measuring the intensities of three control reflections after every 3000 s of exposure time. No significant trend in these intensities was observed during the course of data acquisition. Lorentz and polarization corrections were applied to the data, and the absorption correction factors based on ψ scans were carried out (correction factors 0.91–1.09).

The structure was solved by using Patterson and Fourier methods. Neutral-atom scattering factors (including anomalous scattering) were used.[28] All non-H atoms were refined with anisotropic thermal parameters. Hydrogen atoms were included in calculated positions (C–H = 0.95 Å). Weighted ($w = [\sigma^2(R) + gF^2]^{-1}$) least-squares refinement on F was carried out by alternately refining the cation or the anions plus solvent molecules until the largest shift/esd ratio was equal to 0.02. One of the BF_4 groups was disordered and modeled with groups U and V; refinement gave 45 (3)% occupancy for U and 55 (3)% occupancy for V.

The structure of the cation, $[Fe^{II}_2(N\text{-Et-HPTB})(OBz)]^{2+}$, is shown in Figure 1, together with the numbering scheme for the complex. The final fractional coordinates for **1** are contained in Table S1 (supplementary material), while selected bond lengths and angles for the complex cation are reported in Table II. Complete listings of bond lengths and angles and thermal parameters are included in the supplementary material.

Table II. Selected Bond Lengths (Å) and Angles (deg) for **1**[a]

	a. Bond Lengths		
Fe1–O1	1.973 (7)	Fe2–O1	1.960 (6)
Fe1–O1E	2.056 (7)	Fe2–O2E	2.017 (8)
Fe1–N2	2.318 (8)	Fe2–N1	2.28 (1)
Fe1–N1C	2.07 (1)	Fe2–N1B	2.082 (8)
Fe1–N1D	2.062 (8)	Fe2–N1A	2.07 (1)
O1E–C7E	1.27 (1)	O2E–C7E	1.26 (1)
C2–O1	1.41 (1)	Fe1–Fe2	3.473 (7)
	b. Bond Angles		
O1–Fe1–O1E	98.5 (3)	O1–Fe2–O2E	101.3 (3)
O1–Fe1–N2	79.1 (3)	O1–Fe2–N1	81.0 (3)
O1–Fe1–N1C	121.0 (3)	O1–Fe2–N1B	122.2 (2)
O1–Fe1–N1D	112.1 (4)	O1–Fe2–N1A	108.8 (3)
O1E–Fe1–N2	176.7 (2)	O2E–Fe2–N1	177.6 (3)
N2–Fe1–N1C	76.6 (3)	N1–Fe2–N1B	77.3 (3)
N1C–Fe1–N1D	113.9 (3)	N1B–Fe2–N1A	117.0 (4)
N1D–Fe1–O1E	105.3 (3)	N1A–Fe2–O2E	102.1 (3)
O1E–Fe1–N1C	102.9 (3)	O2E–Fe2–N1B	101.5 (3)
N2–Fe1–N1D	77.7 (3)	N1–Fe2–N1A	76.8 (3)
Fe1–O1–C2	118.6 (6)	Fe2–O1–C2	116.9 (6)
Fe1–O1E–C7E	136.7 (7)	Fe2–O2E–C7E	134.6 (6)
Fe1–O1–Fe2	124.0 (3)	O1E–C7E–O2E	123 (1)

[a] Estimated standard deviations in the least significant digits are given in parentheses.

Methods. NMR spectra were obtained on Varian VXR 300 and VXR 500 spectrometers. The ^1H NMR spectra were obtained using a 90° pulse with 16K data points. An inversion-recovery pulse sequence (180°–τ–90°–AQ) was used to obtain nonselective proton relaxation times (T_1) with carrier frequencies set at several different positions to ensure the validity of the measurements. Temperature calibration for low-temperature ^1H NMR experiments was accomplished with methanol/HCl solutions.[29]

A typical-magnitude ^1H COSY spectrum was collected with 1024 data points in t_2 and 256 data points in t_1 with a bandwidth of 10 kHz and a repetition time of <0.2 s. The time for the data collection for a ~10 mM sample was about 5 h. A 0° shifted sine bell combined with a Gaussian function to give a maximum at one-fourth the acquisition time was applied in both dimensions and zero-filled to 2048 t_2 × 2048 t_1 data points prior to Fourier transformation and symmetrization. In this study, cross signals from pairs of signals with $\Delta\delta$ < 1 ppm in a spectral width of ~30 ppm could be clearly recognized under proper processing procedures.

UV–vis spectra were recorded on an HP 8451A diode array spectrometer. Low-temperature visible spectra were obtained using an immersion dewar equipped with quartz windows. Resonance Raman spectra were collected on a Spex 1403 spectrometer interfaced with a Spex Datamate or DM3000 data collection system using Spectra-Physics Models 2030 argon ion and 375B dye (Rhodamine 6G and DCM) lasers. Spectra were obtained at 79 K using a gold-plated copper cold finger in thermal contact with a dewar containing liquid nitrogen.[30] Raman frequencies were referenced to appropriate solvent features. The Raman excitation profile for the **2**/O_2 adduct was obtained using the 832-cm^{-1} resonance of CD_3CN solvent as an internal standard.

Multifield saturation magnetization data were collected on Quantum Design SQUID susceptometer and fit as described previously.[31] Polycrystalline samples were ground thoroughly and held in place between gel cap halves to give a powder average magnetization in the applied field. No detectable paramagnetic impurities were observed for the gel caps used. The magnetization data were corrected for diamagnetism using the Pascal's constants for the complexes.[32] Theoretical powder average magnetization curves were calculated from the spin Hamiltonian shown in eq 1,[31] where J is the isotropic exchange coupling constant, D_i and E_i

$$\mathcal{H} = J\mathbf{S}_1\cdot\mathbf{S}_2 + \sum[D_i(S_{zi}^2 - 2) + E_i(S_{xi}^2 - S_{yi}^2) + \beta\mathbf{S}_i\cdot\mathbf{g}_i\cdot\mathbf{B}]_{i=1,2} \quad (1)$$

are the axial and rhombic zero-field splitting parameters, and g_i are the g tensors of the uncoupled sites. The saturation magnetization difference data (sample minus control) were fit by the simplex method[33] to find the

(28) *International Tables for X-ray Crystallography*; Kynoch Press: Birmingham, England, 1974; Vol. IV, Tables 2.2 A and 2.3.1.

(29) Van Geet, A. L. *Anal. Chem.* **1970**, *42*, 679–680.

(30) Czernuszewicz, R. C.; Johnson, M. K. *Appl. Spectrosc.* **1983**, *37*, 297–298.

(31) Day, E. P.; Kent, T. A.; Lindahl, P. A.; Münck, E.; Orme-Johnson, W. H.; Roder, H.; Roy, A. *Biophys. J.* **1987**, *52*, 837–853.

(32) Boudreaux, E. A.; Mulay, L. N. *Theory and Applications of Molecular Paramagnetism*; Wiley: New York, 1976.

Table III. Comparison of the Properties of the Diiron(II) Complexes[a]

property	1	4	5	6	7	8
Fe–μ-OR, Å	1.960 (6)	1.984 (2)	1.964 (5)	1.987 (8)	2.052 (1)	2.113 (2)
	1.973 (7)	2.060 (2)	1.993 (5)		2.062 (1)	2.172 (2)
Fe–μ-O_2CR-*O,O'*, Å	2.017 (8)	1.995 (2)	2.071 (5)	2.120 (10)	2.040 (2)	2.067 (3)
	2.056 (7)	2.066 (2)	2.102 (5)	2.142 (9)	2.144 (2)	2.156 (2)
av Fe–N_{arom}, Å	2.07 [5]	2.19 [5]	2.15 [5]		2.20 [6]	2.12 ["5"]
[Fe coord no.]		2.31 [6]				2.14 [6]
Fe···Fe, Å	3.473 (4)	3.684 (1)	3.681 (3)	3.32 (1)	3.348 (1)	3.5936 (8)
Fe–μ-O-Fe, deg	124.0 (3)	131.2 (1)	137.0 (3)	113.2 (2)	108.93 (6)	113.0 (1)
J, cm^{-1} ($\mathcal{H} = JS_1 \cdot S_2$)	21		>0	26	<0	~0.3
ref	this work	23	34	14	16	18

[a] **1** = $[Fe_2(N\text{-Et-HPTB})OBz](BF_4)_2$; **4** = $[Fe_2(6\text{-Me-HPTP})OBz](BF_4)_2$; **5** = $[Fe_2[HB(3,5\text{-}i\text{-}Pr_2pz)_3]_2OH(OBz)]$; **6** = $[Fe_2(Me_3TACN)_2OH(OAc)_2]ClO_4$; **7** = $[Fe_2BPMP(O_2CC_2H_5)_2]BPh_4$; **8** = $[Fe_2(BIPhMe)_2(O_2CH)_4]$.

spin Hamiltonian parameters yielding the minimum in the standard quality of fit parameter, χ^2, where $\chi^2 = \Sigma(\text{moment}_{exp} - \text{moment}_{fit})^2$. The final fits of the data (χ^2 = 17 for **1** and 11 for **3**) were obtained by respectively including 0.93% and 1% monomeric S = 2 (Fe^{II}) impurities, which were subtracted from the raw data. The amount of paramagnetism found from the fitting process was used to scale the vertical axes of the plots.

Dioxygen uptake experiments were conducted on a locally constructed apparatus consisting of a mercury U-tube open at one end to the ambient atmosphere and connected at the other end to a temperature-controlled reaction flask. Typically, 0.1 mmol of diferrous complex was introduced into an O_2-saturated solution; the pressure change resulting from dioxygen uptake was measured, and the number of moles of gas taken up was calculated using the ideal gas law.

The reactions of $\mathbf{1}/O_2$ and $\mathbf{3}/O_2$ (0.02-mmol scale) with 2,4-di-*tert*-butylphenol or Ph_3P (10-fold excess) were conducted at −50 °C in CH_2Cl_2/DMSO (9:1 v/v) over a 2-h period; excess O_2 was removed after adduct formation. The amount of product formed (3,3′,5,5′-tetra-*tert*-butyl-2,2′-biphenol or $OPPh_3$, respectively) was determined by NMR integration.

Results

The functions of Hr, MMO, and RNR depend on the interaction of a diferrous center with dioxygen. While oxyHr has been characterized to have a (μ-oxo)bis(μ-carboxylato)diferric unit with a terminally ligated hydroperoxide,[3] the nature of putative O_2 adducts for the RNR R2 and MMO reaction cycles has not been established. In our efforts to model the chemistry of these diiron–oxo proteins, we have explored the use of dinucleating ligands which utilize a 2-hydroxypropane unit to link two tridentate N_3 ligands to synthesize diferrous complexes that bind O_2. These efforts have resulted in the isolation and characterization of $[Fe^{II}_2L(OBz)]X_2$ complexes (**1**, L = *N*-Et-HPTB; **2**, L = HPTB; **3**, L = HPTP). In the following, we discuss the structural, spectroscopic, and reactivity properties of these diferrous complexes and their O_2 adducts.

Crystal Structure of $[Fe^{II}_2(N\text{-Et-HPTB})(O_2CC_6H_5)](BF_4)_2 \cdot 3CH_3CN$. The structure of $[Fe^{II}_2(N\text{-Et-HPTB})(OBz)](BF_4)_2$ (Figure 1) shows two iron centers bridged by the alkoxo oxygen atom of *N*-Et-HPTB and by a benzoate ligand and terminally coordinated by nitrogen atoms from the dinucleating ligand. Each iron atom has approximately trigonal bipyramidal geometry with the amine nitrogens and benzoate oxygens as the axial ligands. A closely related structure is that of $[Cu_2(N\text{-Et-HPTB})(OAc)](ClO_4)_2$, with the cupric ions in approximately trigonal bipyramidal coordination sites and a very similar ligand arrangement.[25]

The structure of **1** is compared with those of other diferrous complexes in Table III. Closely related is a structure recently reported by Suzuki et al.[23] wherein the pendant benzimidazoles of **1** are replaced with 6-methylpyridyl moieties; the structure of $[Fe_2(6\text{-Me-HPTP})(OBz)(H_2O)](BF_4)_2$ (**4**) differs from that of **1** in having an additional water molecule coordinated to one of the iron centers, affording a complex with one 6-coordinate and one 5-coordinate iron center. Another closely related structure is that of $[Fe_2[HB(3,5\text{-}i\text{-}Pr_2pz)_3]_2OH(OBz)]$ (**5**) reported by Kitajima et al.,[34] which has two 5-coordinate ferrous centers

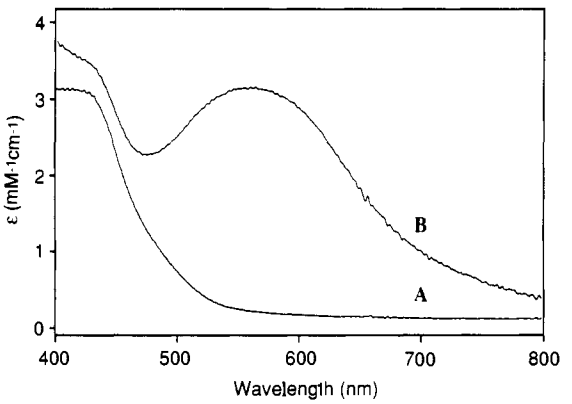

Figure 2. UV–vis spectra of **3** (A) and $\mathbf{3}/O_2$ (B) in CH_2Cl_2/DMSO (9:1 v/v) at −80 °C.

bridged by hydroxide and benzoate. Also listed are the relevant structural parameters for complexes with tribridged (μ-OR)bis(μ-carboxylato)diiron(II) cores, such as $[Fe_2(OH)(OAc)_2(Me_3TACN)_2]ClO_4$ (**6**)[14] $[Fe_2(BPMP)(O_2CC_2H_5)_2]BPh_4$ (**7**),[16] and $[Fe_2(BIPhMe)_2(HCO_2)_4]$ (**8**).[18]

A comparison of the core dimensions of the diferrous complexes in Table III reveals some interesting trends. The average Fe–μ-O distances for these complexes in general reflect the basicity of the μ-OR groups with shorter distances corresponding to higher basicity, i.e. OH ~ O–alkyl < OPh < O_2CR for $r_{Fe-\mu-O}$. There are large differences in the two Fe–μ-O bonds of **4** and **8** which arise from the presence of 5- and 6-coordinate centers in these two complexes. Complexes **1**, **4**, and **5**, all of which have dibridged cores, have Fe–O–Fe angles significantly larger than those of tribridged **6**–**8**. This is most likely an effect of the number of carboxylate bridges on the Fe–O–Fe angle, which has previously been noted in (μ-oxo)diferric complexes.[35] Steric interactions are probably responsible for making the Fe–O–Fe angles in **4** and **5** even larger than that of **1**. The combination of the above factors affords an Fe–Fe distance of 3.473 (4) Å for **1**, which is intermediate between those of **4** and **5** (3.7 Å) and those of **6** and **7** (3.3 Å). This range of distances demonstrates the flexibility of carboxylates in a bridging dinuclear unit. The Fe–N_{arom} bond distances of **1** are the shortest found in the diferrous series. The short distance reflects the 5-coordinate nature of the iron environment and the basicity of the ligands.

Properties of the Diferrous Precursors. The diferrrous complexes are air-sensitive light yellow solids, the colors of which arise from UV absorption tails. **1** and **3** exhibit intense UV bands in CH_3CN at 330 nm (ϵ_M 2400) and 312 nm (ϵ_M 6200), respectively, but no significant visible absorption (Figure 2). The lack of low-energy visible absorption bands despite the presence of aromatic nitrogen ligands suggests that these are high-spin ferrous complexes. Indeed, the Mössbauer parameters of **1** (δ = 1.07

(33) Nelder, J.; Mead, R. *Comput. J.* **1965**, 308–313.

(34) Kitajima, N.; Tamura, N.; Tanaka, M.; Moro-oka, Y. *Inorg. Chem.* **1992**, *31*, 3342–3343.

(35) Norman, R. E.; Yan, S.; Que, L., Jr.; Backes, G.; Ling, J.; Sanders-Loehr, J.; Zhang, J. H.; O'Connor, C. J. *J. Am. Chem. Soc.* **1990**, *112*, 1554–1562.

Table IV. ^{1}H NMR Data[a] for Complexes **1** and **3**

signal[b]	1[c]	1[d]	3[c]	3[d]	3[e]	3[c] + 50 equiv of Ph_3PO
CH	178.4 (0.8)	166.2 (0.7)	203.4 (1.1)	151.0 (0.9)	137.1	142.1
CH_2	152.4 (2.8)	144.3 (2.6)	146.1 (3.4)	116.6 (3.1)	112.2	111.4
CH_2	105.8 (2.9)	101.8 (2.6)	70.0 (2.3)	101.6 (2.3)	109.0	101.9
CH_2	78.1 (3.0)	64.2 (2.5)	57.3 (2.8)	78.0 (3.1)	84.6	76.9
CH_2	55.1 (1.7)	50.5 (1.6)	49.3 (2.3)	46.0 (1.5)	45.5	40.7
CH_2	34.6 (1.6)	41.2 (1.6)	44.6 (2.5)	33.5 (1.8)	28.0	30.0
CH_2	−8.8 (1.5)	−7.5 (1.6)	9.2	−16.8 (1.3)	−23.8	−22.7
α	18.3 (1.0)	14.8 (1.5)	107.3 (1.1)	103.5 (1.2)	105.0	103.8
β	7.3 (21)	6.6 (22)	43.9 (13)	44.3 (13)	44.0	44.5
			42.9 (15)	43.8 (14)	44.0	44.1
γ	4.5 (53)	4.2 (46)	−2.9 (33)	−0.21 (29)	3.2	2.8
δ	20.6 (37)	19.6 (35)				
a	8.6 (18)	7.3 (19)				
b	7.4 (21)	6.0 (21)				
c	0.1 (30)	0.0 (29)				
α′	22.5 (3.6)	22.8 (3.8)	92.7 (1.0)	92.3 (1.2)	92.1	92.9
β′	1.9	1.9	41.8 (16)	40.9 (14)	40.8	40.7
			41.0 (17)	38.4 (16)	37.9	37.9
γ′	1.6 (61)	1.7	−3.7 (37)	1.9	0.6	0.9
δ′	20.8 (36)	20.2 (36)				
a′	11.3 (19)	10.1 (19)				
b′	12.5 (28)	11.2 (20)				
c′	4.0 (32)	3.6 (32)				
o	13.7 (1.5)	14.8 (1.5)	13.9 (5.0)	17.2 (4.5)	17.3	16.5
m	12.5 (28)	12.4 (35)	10.3 (50)	10.8 (46)	10.7	12.0
p	13.0 (60)	13.2 (58)	9.5 (54)	12.0 (97)	12.4	14.2

[a] Shift in ppm (T_1 in ms). [b] Greek letters designate positions on the benzimidazole or pyridine rings; a, b, and c designate the diastereoptic CH_2 and CH_3 protons of the *N*-ethyl groups of *N*-Et-HPTB, respectively; and o, m, and p designate positions on the benzoate. [c] In CD_3CN. [d] In CD_3CN/DMSO-d_6 (9:1 v/v). [e] In CD_3CN/DMSO-d_6 (1:1 v/v).

mm/s relative to Fe metal at 298 K, ΔE_Q = 3.13 mm/s)[22] support this assignment.

Magnetization data of polycrystalline samples of **1** and **3** were collected at fixed fields of 0.078, 1.0, and 5.0 T, over the temperature range 2–300 K. The data sets are plotted as molar susceptibility (χ_{mol}) versus inverse temperature at the three fields (Figure 3). The maxima in the plots at ~70 K for **1** and ~85 K for **3** are indicative of *antiferro*magnetic coupling. Futhermore, the nesting of the magnetization curves with the lowest field data having the largest values at low temperatures is also characteristic of an antiferromagnetically coupled diferrous complex with zero-field splitting and saturation magnetization.[36] The solid lines are least-squares fits calculated by diagonalization of the 25 × 25 matrix representation for the spin Hamiltonian of eq 1 under the assumption of isotropic g values and equal and coaxial $\mathbf{D}_i$ tensors. The final parameter sets of the best fits are as follows: for **1**, J = 21.0 (2) cm^{-1}, $|D_i|$ = 8.9 (5) cm^{-1}, E_i/D_i = 0.11 (4), and g_i = 2.06 (3); for **3**, J = 24.9 (2) cm^{-1}, $|D_i|$ = 10.1 (5) cm^{-1}, E_i/D_i = 0.07 (4), and g_i = 2.16 (3). The values of J obtained for **1** and **3** are comparable to that reported for $[Fe_2(OH)(OAc)_2(Me_3TACN)_2]ClO_4$ (26 cm^{-1}),[14b] consistent with the notion that hydroxo and alkoxo bridges with similar geometries mediate coupling interactions of comparable magnitude and that these single-atom bridges are the principal pathways for the antiferromagnetic coupling in these systems.

The NMR spectra of **1** and **3** (Figures 4 and 5) display relatively sharp well-resolved resonances due to the very favorable electronic relaxation time of the ferrous centers.[37] The peaks are spread over a 200 ppm range. Most of the protons can be assigned by a comparison of T_1 values and COSY connectivities (Table IV); the COSY information is particularly useful for identifying the ring protons of the pendant ligands and the bridging benzoate.

All the CH_2 and CH protons are observed. The sole methine proton, being geminal to the bridging alkoxide, is readily assigned by its single-proton integration, large shift, and very short T_1 value due to its proximity to the metal centers. The methylene protons appear as six resonances with slightly longer T_1 values and two-proton integrations each; the number of resonances observed suggests that there is an apparent plane of symmetry relating the halves of the molecule. The six CH_2 resonances would thus arise in the half-molecule from the two protons on the hydroxypropane

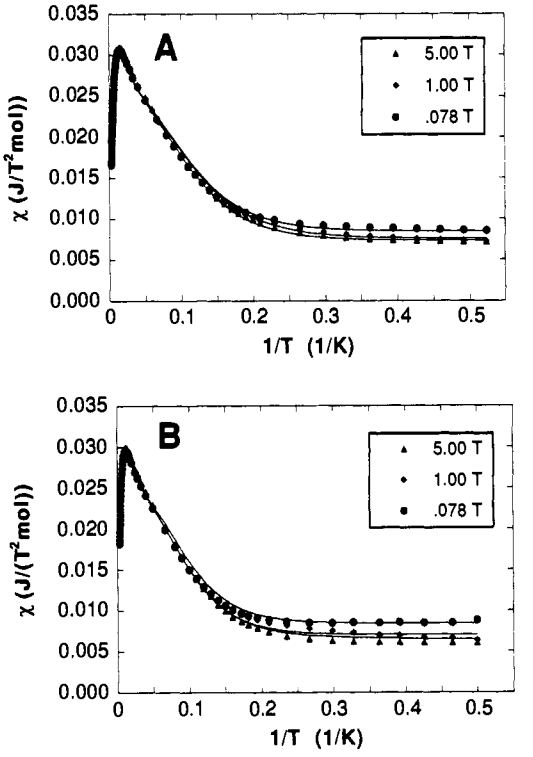

Figure 3. Temperature dependence of the magnetic susceptibility of **1**, $[Fe_2(N\text{-Et-HPTB})OBz](BF_4)_2$, (A) and **3**, $[Fe_2(HPTP)OBz](BPh_4)_2$, (B) at three fields over the temperature range 2–300 K. Data are plotted as molar susceptibility (χ_{mol}) versus inverse temperature. The solid lines are least-squares fits calculated by diagonalization of the 25 × 25 matrix representation for the spin Hamiltonian of eq 1 under the assumption of isotropic g values and equal and coaxial $\mathbf{D}_i$ tensors. Final parameter sets for fits shown are as follows: for **1**, J = 21.0 (2) cm^{-1}, $|D_i|$ = 8.9 (5) cm^{-1}, E_i/D_i = 0.11 (4), and g_i = 2.06 (3); for **3**, J = 24.9 (2) cm^{-1}, $|D_i|$ = 10.1 (5) cm^{-1}, E_i/D_i = 0.07 (4), and g_i = 2.16 (3).

(36) Wiegel, J. A.; Srivastava, K. K. P.; Day, E. P.; Münck, E.; Holm, R. H. *J. Am. Chem. Soc.* **1990**, *112*, 8015–8023.
(37) Ming, L.-J.; Jang, H. G.; Que, L., Jr. *Inorg. Chem.* **1992**, *31*, 359–364.

Table V. Electronic and Vibrational Features of the O_2 Adducts and Related Diferric Peroxide Complexes

compound	λ_{max} (ϵ), nm (M^{-1} cm^{-1})	ν(Fe–O) (^{18}O), cm^{-1}	ν(O–O) (^{18}O), cm^{-1}	binding mode	ref
$1/O_2$ in CH_2Cl_2	588 (1500)	476 (460)	900 (850)	μ-1,2	this work
$3/O_2$ in CH_2Cl_2/DMSO (9:1 v/v)	562 (3200)				this work
$3/O_2$ in CH_3CN/DMSO (8:2 v/v)	572 (2060)	453, 481 (444)	877, 893 (834)	μ-1,2	this work
Fe_2(HPTB)OH$(NO_3)_4/H_2O_2$	560 (2200)	476 (457)	895 (854)	μ-1,2	42
[Fe[HB(3,5-*i*-Pr_2pz)$_3$](OBz)]$_2O_2$	679	418 (409)	876 (827)	μ-1,2	21
[Fe_2[HB(3,5-*i*-Pr_2pz)$_3$]$_2$OH(OBz)]O_2	700				34
[Fe_2(5-Me-HXTA)(O_2)(OAc)]$^{2-}$	480 (2370)	n.o.	884	μ-1,2	40
[[Fe($Ph_3PO)_4]_2O_2]^{4+}$	576 (3540)	n.o.	882 (848)	μ-1,2 (?)	43
[Fe(OEP)O_2]$^-$		n.o.	806 (759)	η^2	44
[Fe^{III}(EDTAH)O_2]$^{2-}$	520 (530)	n.o.	815	η^2	39
[$Fe_6(O)_2(O_2)$(OBz)$_{12}$(OH_2)$_2$]	534 (1590)	n.r.	853	μ_4	45
oxyhemerythrin	500 (2300)	503 (480)	844 (797)	η^1	10

backbone and the four protons associated with the benzimidazole arms. Their individual isotropic shifts reflect the orientation of the C–H bond in the chelate rings (i.e. whether pseudoaxial or pseudoequatorial) which modulates the amount of spin delocalization.[37,38]

The COSY spectrum of **1** in CD_3CN (Figure 4) shows a number of cross peaks and identifies the various multispin systems present in the complex. For instance, the protons of the *N*-ethyl group form an ABX_3 spin system, while the β, γ, and δ protons of the benzimidazole constitute an AMX unit. Unfortunately, the benzimidazole α protons are too close to the metal centers and have T_1 values too short to permit its connectivity to the corresponding β proton to be observed; we assign them to remaining broad features with appropriately short T_1 values. The benzoate protons are readily recognized by their T_1 values and the correlation between meta and para protons. Assignments for the resonances associated with **3** are made following a similar strategy (Table IV).

The addition of DMSO-d_6 to the CD_3CN solutions of **1** and **3** effects a substantial change in their NMR spectra (Figure 5, Table IV). All the aliphatic CH_2 and methine protons exhibit significant changes in isotropic shift, indicating alterations in the conformations of the chelate rings. The benzimidazole, pyridine, and benzoate protons are also affected but to a lesser extent. Titration experiments show that these changes occur as the DMSO concentration increases and maximize when the solvent is 50% DMSO (v/v). A similar effect is observed with the titration of solutions of **3** with $OPPh_3$, with the maximum change observed at 50 equiv (Table IV); in contrast, PPh_3 has no effect. Note the patterns of the peaks in the 100–200 ppm region and the pyridine β peaks near 40 ppm for the spectra of **3** in Figure 5; the similarities of the spectra derived from DMSO and Ph_3PO addition suggest that analogous changes are occurring. The smooth transition from one form to another suggests the coordination of the added ligand to the available sites in these complexes, which occurs under conditions of fast exchange on the NMR time scale. The ^{31}P NMR signal of the added $OPPh_3$ cannot be found in the ^{31}P NMR spectrum, while the resonance due to the phosphine is clearly observed at its expected diamagnetic position in the presence of **3**; these observations suggest that the ^{31}P resonance of the phosphine oxide is absent due to broadening and shifting brought about by coordination to the diferrous complexes. By inference, DMSO seems also likely to coordinate to the diferrous unit, thereby converting the trigonal bipyramidal metal centers into 6-coordinate centers. The increase in coordination number necessitates some movement of the pendant ligands, thus engendering the conformational effects indicated by the isotropic shift changes.

Spectroscopic Characterization of the Dioxygen Adducts. The diferrous complexes **1**–**3** bind O_2 irreversibly, and the resulting intermediates can be stabilized at low temperature to allow their spectroscopic characterization. Exposure of a CH_2Cl_2 solution of **1** to O_2 at −60 °C affords a species with an intense purple-blue

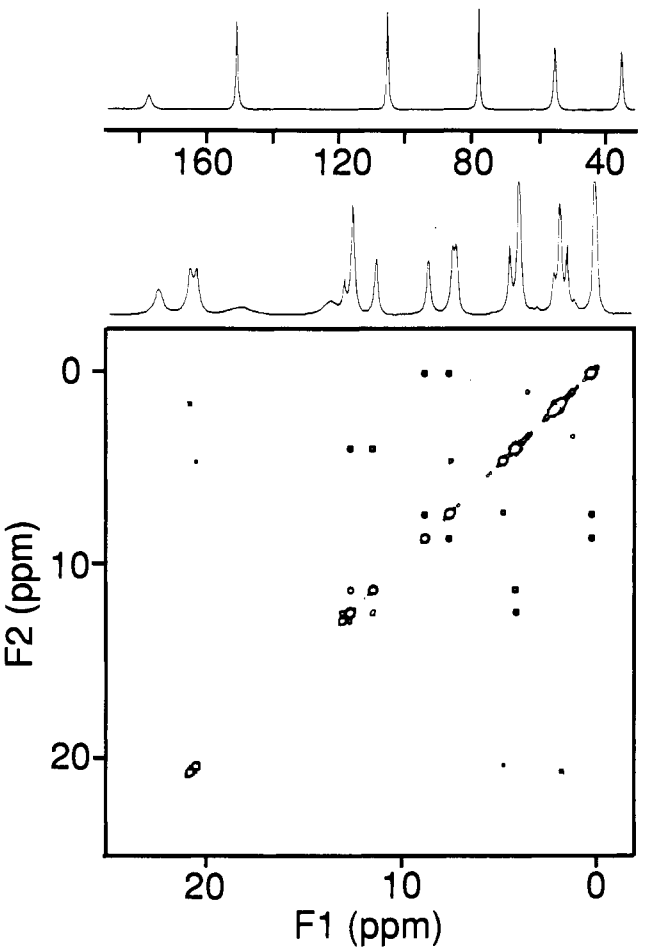

Figure 4. ^1H NMR spectrum of **1** in CD_3CN and its COSY spectrum in the −5 to +25 ppm region.

color corresponding to a visible band at 588 nm. Application of a vacuum does not affect the stability of the complex, indicating irreversible adduct formation. Similar observations are made for the $3/O_2$ adduct in CH_2Cl_2/DMSO (9:1), which exhibits a λ_{max} at 562 nm (Figure 2). Manometric measurements of O_2 uptake for **1** and **3** show that one O_2 molecule binds per diferrous center. Dioxygen presumably binds to the open coordination sites of the diferrous complex and is reduced to the peroxide oxidation state by the iron centers.

When compared to those of other diferric peroxide complexes (Table V), the absorption maxima of the three adducts near 600 nm are intermediate between those of [Fe[HB(3,5-*i*-Pr_2pz)$_3$]-OBz]$_2O_2$ and [Fe_2[HB(3,5-*i*-Pr_2pz)$_3$]$_2$OH(OBz)(O_2)] near 700 nm[21,34] and those of [Fe(EDTA)O_2]$^{4-}$ and [Fe_2(5-Me-HXTA)(OAc)(O_2)]$^{2-}$ near 500 nm.[39,40] This progression reflects

(38) Holm, R. H.; Hawkins, C. J. In *NMR of Paramagnetic Molecules, Principles and Applications*; La Mar, G. N., Horrocks, W. DeW., Jr., Holm, R. H., Eds.; Academic: New York, 1973; Chapter 7.

(39) Ahmad, S.; McCallum, J. D.; Shiemke, A. K.; Appelman, E. H.; Loehr, T. M.; Sanders-Loehr, J. *Inorg. Chem.* **1988**, *27*, 2230–2233.

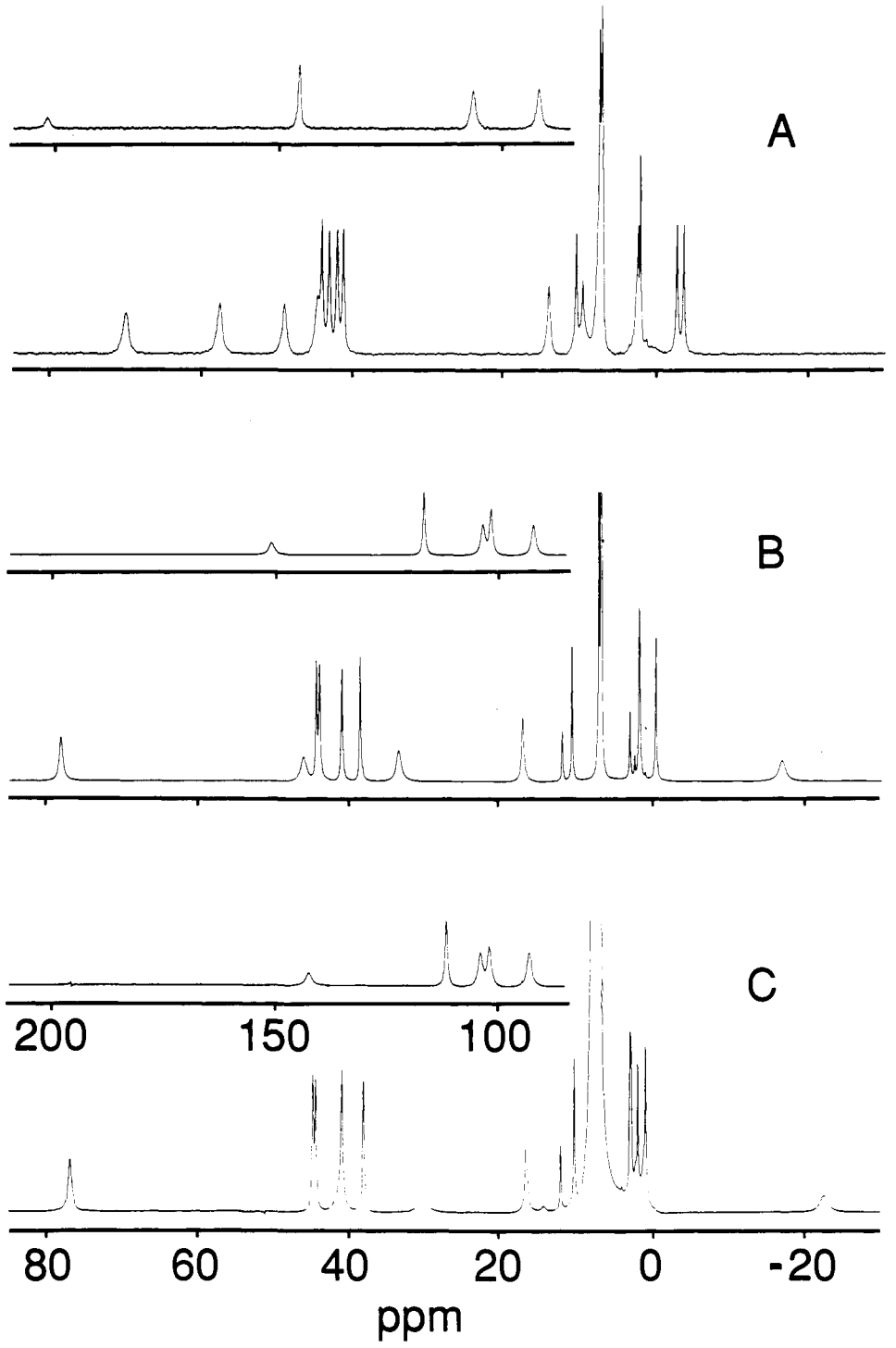

Figure 5. ^{1}H NMR spectra of **3** (A) in CD_3CN, (B) in CD_3CN/DMSO-d_6 (9:1 v/v) and (C) in CD_3CN with 50 equiv of Ph_3PO.

the intermediate Lewis acidity of the Fe(III) centers in the adducts of **1–3**, which are sandwiched between complexes with weakly basic pyrazoles on one end and those that are carboxylate-rich on the other, and suggests that the chromophore arises from a peroxo-to-Fe(III) charge-transfer transition.

The nature of the bridging carboxylate also affects the λ_{max} of the O_2 adduct. When the corresponding diferrous propionate complex of **1** is exposed to O_2, λ_{max} of the adduct shifts to 570 nm (vs 588 nm). This shift indicates that the carboxylate remains coordinated upon adduct formation. The presence of the more basic propionate would be expected to render the iron centers less Lewis acidic and thereby blue-shift the peroxide-to-Fe(III) charge-transfer transition as observed.

The resonance Raman spectra of the dioxygen adducts verify that the new spectral feature at ca. 580 nm is a peroxide-to-iron(III) charge-transfer transition (Figure 6, Table V). For **1**/O_2 with 575-nm excitation at 79 K, two features at 476 and 900 cm^{-1} are observed; the first is assigned to ν(Fe–O), while the other, which appears as a Fermi doublet, is assigned to ν(O–O). Accordingly, these shift to 460 and 850 cm^{-1}, respectively, with the use of $^{18}O_2$, in good agreement with the calculated shifts predicted using a simple diatomic model (ν(Fe–^{18}O) 455 cm^{-1}; ν(^{18}O–^{18}O) 849 cm^{-1}). The Fermi doublet observed for ν(O–O) also collapses into a single peak upon ^{18}O substitution. Similarly for the **3**/O_2 adduct, the ν(Fe–O) and ν(O–O) features appear as Fermi doublets at 481 and 453 cm^{-1} and at 893 and 877 cm^{-1}, respectively; these shift to 444 cm^{-1} (ν_{calcd} 446 cm^{-1}) and 834 cm^{-1} (ν_{calcd}

(40) (a) Murch, B. P.; Bradley, F. C.; Que, L., Jr. *J. Am. Chem. Soc.* **1986**, *108*, 5027–5028. (b) Murch, B. P. Ph.D. Thesis, Cornell University, 1987.

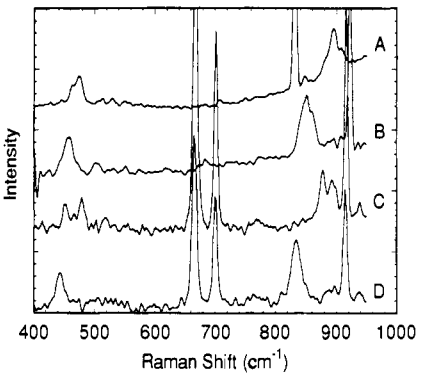

Figure 6. Resonance Raman spectra of (A) $1/^{16}O_2$ in CD_3CN, (B) $1/^{18}O_2$ in CH_3CN, (C) $3/^{16}O_2$ in CH_3CN/DMSO (4:1 v/v), and (D) $3/^{18}O_2$ in CH_3CN/DMSO (4:1 v/v). Spectra shown are the average of 5–10 scans obtained on frozen solutions at ~80 K with laser excitation at 580–600 nm, 200-mW power, and 4-cm^{-1} slits. Off-scale features in the spectra arise from solvent vibrations.

834 cm^{-1}), respectively, when $^{18}O_2$ is used.

An excitation profile study of the ν(O–O) feature of the $1/O_2$ adduct shows that its intensity varies with excitation wavelength, confirming the assignment of the 588-nm band as a peroxide-to-iron charge-transfer transition; however, the excitation wavelength at which maximum enhancement is observed is somewhat red-shifted from the absorption maximum (640 vs 588 nm). Such differences between Raman excitation maxima and absorption maxima have been noted for a number of synthetic iron complexes.[41]

When compared with those observed for other peroxoiron complexes (Table V), the resonance Raman spectra of the O_2 adducts suggest that O_2 is bound as a μ-1,2-peroxo unit. Both $1/O_2$ and $3/O_2$ adducts have ν(O–O) values near 900 cm^{-1}, just like other complexes with proposed μ-1,2-peroxo moieties.[21,40,42,43] In contrast, η^2-peroxo complexes have ν(O–O) values near 800 cm^{-1},[39,44] while oxyhemerythrin (η^1-hydroperoxo) and $[Fe_6(O)_2(O_2)(OBz)_{12}(OH_2)_2]$ (μ_4-peroxo) have ν(O–O) values near 850 cm^{-1}.[10,45] Recent calculations for copper–peroxo model systems indicate that the energy of the peroxide bond is related to the peroxide binding mode; *cis*- and *trans*-μ-1,2-peroxo bridges are calculated to have similar O–O bond energies, while μ-η^2,η^2-peroxo species should have somewhat weaker values.[46] It appears that these results may apply to the iron peroxide complexes as well, as the μ-1,2-peroxo complexes exhibit higher ν(O–O) values than the η^2-peroxo complexes (assuming the η^2 mode has bonding interactions similar to those of the μ-η^2,η^2 mode).

The $1/O_2$ and $2/O_2$ adducts exhibit NMR spectra that provide further insight into the electronic structure of these complexes; unfortunately, the $3/O_2$ adduct affords a spectrum too broad to yield any useful information. The spectrum of $2/O_2$ in CD_3CN/acetone-d_6 at −60 °C shows the NH protons at 23 and 25 ppm and the C7 benzimidazole protons at ~17 ppm. These assignments are based on solvent exchangeability properties and T_1 values. The corresponding protons of the Fe_2(OH)HPTB-$(NO_3)_4/H_2O_2$ adduct are found at 25 °C at 26 and 28 ppm and at 17 ppm, respectively.[42] For comparison, the corresponding protons in Fe_2(OH)HPTB$(NO_3)_4$ (J = 44 cm^{-1}) are found at 44 and 48 ppm and at 35 ppm, respectively,[42] while those of $[Fe_4O_2(HPTB)_2(OBz)_2]X_4$ (J > 200 cm^{-1}) are found at 14 and 16 ppm and at 9.5 and 12.3 ppm, respectively.[26] Since these complexes all contain diferric HPTB moieties, the isotropic shifts of corresponding protons reflect the strength of the antiferromagnetic coupling interaction.[47] We thus estimate $J \sim 140 \pm 20$ cm^{-1} for the O_2 adduct, very similar to that estimated for the Fe_2(OH)HPTB$(NO_3)_4/H_2O_2$ adduct.

The value of J estimated for the $2/O_2$ adduct is larger than that expected for a diferric complex with an alkoxo bridge alone or one with both an alkoxo and a μ-1,1-peroxo bridge. $[Fe_2(HPTB)\{O_2P(OPh)_2\}Cl_2(MeOH)]^{2+}$, an example of a ($\mu$-alkoxo)diferric complex, exhibits a J of 28 cm^{-1},[48] while complexes with $Fe_2(OR)_2$ cores typically have J values of 20–50 cm^{-1}.[49] The larger J value suggests a peroxo coordination mode that provides an additional coupling pathway. 1,2-Peroxo bridges are known to mediate strong antiferromagnetic coupling; for example, the structurally characterized O_2 adduct $\{[Cu(TPA)]_2(\mu\text{-}1,2\text{-}O_2)\}X_2$ is nearly diamagnetic,[50] while $[Fe(TMP)]_2(\mu\text{-}1,2\text{-}O_2)$ has been estimated by NMR to have a J value of approximately 200 cm^{-1}.[51] The dioxygen moieties in both complexes have trans μ-1,2-binding modes, a conformation that is expected to afford the maximum coupling interaction by analogy to the Karplus relation governing vicinal ^1H–^1H coupling constants. In contrast, the dioxygen moiety in the $2/O_2$ adduct would likely be contrained to a cis μ-1,2 mode. An M–O–O–M dihedral angle of 0° would also be expected to afford the maximum coupling interaction; however, it is likely that the M–O_2–M units in the O_2 adducts of **1**–**3** will have nonzero dihedral angles as found for the corresponding unit in the tribridged $[Co(BPMP)(OBz)O_2](BF_4)_2$ (51°).[52] The nonzero dihedral angles required by the tribridged (μ-alkoxo)(μ-1,2-peroxo)(μ-carboxylato)diiron structure would be expected to engender the slightly smaller antiferromagnetic coupling observed for the adducts in this paper.

Stability and Reactivity of the Dioxygen Adducts. The dioxygen adducts reported in this study exhibit differing stabilities and reactivity properties. While the $1/O_2$ and $2/O_2$ adducts are indefinitely stable in CH_2Cl_2 at −60 °C, the $3/O_2$ adduct cannot be formed in CH_3CN at −40 °C, as noted by Suzuki et al.,[23] or in CH_2Cl_2 even at −80 °C. The presence of DMSO, however, greatly stabilizes all the adducts. For $3/O_2$ the addition of 10% DMSO to CH_2Cl_2 allows the adduct to form at −80 °C and persist for hours at that temperature. Similarly, the addition of 20% DMSO to CH_3CN promotes the formation of the $3/O_2$ adduct at −60 °C, but the adduct begins to decompose slowly almost immediately. More dramatically, the presence of DMSO allows the $1/O_2$ and $2/O_2$ adducts to form and persist for ~30 min even at ambient temperature. The adducts are similarly affected by the addition of other polar aprotic solvents like *N*,*N*-dimethylformamide and *N*,*N*-dimethylacetamide or triphenylphosphine oxide, suggesting that a more polar solvent environment stabilizes the O_2 adducts.

The differing stabilities of the (μ-1,2-peroxo)diiron(III) complexes are also reflected in their reactivities toward potential substrates. $1/O_2$ is rather unreactive; its visible spectrum is unaffected by the addition of 2,4-di-*tert*-butylphenol or Ph_3P at −50 °C over a 2-h period. Upon warming and adduct decomposition, there is no evidence for the formation of the corresponding

(41) Sanders-Loehr, J.; Wheeller, W. D.; Shiemke, A. K.; Averill, B. A.; Loehr, T. M. *J. Am. Chem. Soc.* **1989**, *111*, 8084–8093.
(42) Brennan, B. A.; Chen, Q.; Juarez-Garcia, C.; True, A. E.; O'Connor, C. J.; Que, L., Jr. *Inorg. Chem.* **1991**, *30*, 1937–1943.
(43) Sawyer, D. T.; McDowell, M. S.; Spencer, L.; Tsang, P. K. S. *Inorg. Chem.* **1989**, *28*, 1166–1170.
(44) McCandlish, E.; Miksztal, A. R.; Nappa, M.; Sprenger, A. G.; Valentine, J. S.; Stong, J. D.; Spiro, T. G. *J. Am. Chem. Soc.* **1980**, *102*, 4268–4271.
(45) Micklitz, W.; Bott, S. G.; Bentsen, J. G.; Lippard, S. J. *J. Am. Chem. Soc.* **1989**, *111*, 372–374.
(46) Ross, P. K.; Solomon, E. I. *J. Am. Chem. Soc.* **1991**, *113*, 3246–3259.
(47) (a) Maroney, M. J.; Kurtz, D. M., Jr.; Nocek, J. M.; Pearce, L. L.; Que, L., Jr. *J. Am. Chem. Soc.* **1986**, *108*, 6871–6879. (b) Que, L., Jr.; Maroney, M. J. *Met. Ions Biol. Syst.* **1987**, *21*, 87–120.
(48) Bremer, B.; Schepers, K.; Fleischhauer, P.; Haase, W.; Henkel, G.; Krebs, B. *J. Chem. Soc., Chem. Commun.* **1991**, 510–511.
(49) (a) Thich, J. A.; Oh, C. C.; Powers, D.; Vasilou, B.; Mastropaolo, D.; Potenza, J. A.; Schugar, H. J. *J. Am. Chem. Soc.* **1976**, *98*, 1425–1433. (b) Borer, L.; Thalken, L.; Ceccarelli, C.; Glick, M.; Zhang, J. H.; Reiff, W. M. *Inorg. Chem.* **1983**, *22*, 1719–1724. (c) Chiari, B.; Piovesana, O.; Tarantelli, T.; Zanazzi, P. F. *Inorg. Chem.* **1982**, *21*, 2444. (d) Walker, J. D.; Poli, R. *Inorg. Chem.* **1990**, *29*, 756–761. (e) Ménage, S.; Que, L., Jr. *Inorg. Chem.* **1990**, *29*, 4293–4297.
(50) Jacobson, R. R.; Tyeklar, Z.; Farooq, A.; Karlin, K. D.; Liu, S.; Zubieta, J. *J. Am. Chem. Soc.* **1988**, *110*, 3690–3692.
(51) Balch, A. L.; Chan, Y.-W.; Cheng, R.-J.; La Mar, G. N.; Latos-Grazynski, L.; Renner, M. *J. Am. Chem. Soc.* **1984**, *106*, 7779–7785.
(52) Suzuki, M.; Ueda, I.; Kanatomi, N.; Murase, I. *Chem. Lett.* **1983**, 185–188.

biphenol, but 0.1 equiv of $OPPh_3$ is detected by ^{31}P NMR. In contrast, 2,4-di-*tert*-butylphenol and PPh_3 accelerate the decomposition of $3/O_2$ at −50 °C, while styrene and cyclohexene have no effect. The 2,4-di-*tert*-butylphenol reaction affords 0.5 mol of the biphenol/mol of diferrous complex, while the PPh_3 reaction yields 0.6 equiv of $OPPh_3$. Thus, about half of the oxidizing equivalents implied by the bound peroxide can be intercepted in the case of $3/O_2$. The adduct with pendant pyridines is clearly more reactive than the corresponding complex with pendant benzimidazoles; these differences in reactivity suggest that the pyridine ligands enhance the electrophilic character of the bound dioxygen.[53] However, further investigations are needed to clarify the factors that affect the reactivity of the bound dioxygen.

Discussion

Using dinucleating ligands that contain the 2-hydroxypropane backbone, we have synthesized and characterized diferrous complexes (**1–3**) that generate dioxygen adducts upon exposure to air. These complexes differ from previously reported diferrous complexes in having readily accessible coordination sites that permit the formation of dioxygen adducts. Complexes **6** and **7** have coordinatively saturated Fe(II) centers which autoxidize upon exposure to O_2.[14,16] Complex **8** suffers a similar fate, despite the apparent availability of a coordination site on one Fe(II) center; the carbonyl oxygen of the monodentate bridging formate interacts weakly with the nominally 5-coordinate Fe(II) center (r_{Fe-O} = 2.7 Å) and appears to block access to the "vacant" site.[18] The accessibility of the vacant sites in **1–3** is also indicated by the dramatic changes observed in the NMR spectra of the complexes upon addition of DMSO or $OPPh_3$. Subsequent to our initial report of **1**,[22] two other diferrous complexes were reported to bind O_2;[23,24] these complexes have available coordination sites as well. This requirement for site accessibility is a principle well established in the chemistry of dioxygen binding previously demonstrated for biomimetic heme and copper complexes.

Exposure of **1–3** to O_2 leads to irreversible adduct formation, in contrast to the reversible O_2-binding chemistry observed for **4**[23] and $[LFe(OBz)(CH_3CN)]$.[21] A comparison of **3** and **4** is particularly instructive, since the dinucleating ligands used in these complexes merely differ by the presence of 6-methyl groups on the pendant pyridines. The irreversibility of O_2 binding in the case of **3** indicates that the diferric state is strongly favored relative to the diferrous state, but the presence of 6-methyl groups in **4** appears to alter the balance to favor reversibility. The introduction of 6-methyl groups on pendant pyridines of tripodal ligands has been shown to shift the redox potential of the metal center to more positive values, because steric interactions prevent the pyridine nitrogens from approaching the metal center as closely.[54,55] The redox potential of $[LFe(OBz)(CH_3CN)]$ may also favor reversibility because of the presence of pyrazoles which are less basic than the benzimidazoles and pyridines found in **1–3**. Another factor that may promote reversibility of O_2 binding is the presence of a hydrophobic pocket surrounding the putative O_2-binding site as provided by the methyl groups in **4** and the isopropyl groups in $[LFe(OBz)(CH_3CN)]$.

The accumulated spectroscopic results discussed earlier suggest that the dioxygen adducts of **1–3** have tribridged (μ-1,2-peroxo)(μ-carboxylato)(μ-alkoxo)diferric cores, analogous to that structurally characterized in a dicobalt complex, $[Co_2(bpmp)(OBz)O_2](BF_4)_2$, which has a μ-phenoxo group in place of the alkoxo bridge.[52] This (μ-1,2-peroxo)diiron structure is clearly distinct from that found for oxyhemerythrin, which has a terminal hydroperoxide coordinated to one of the iron centers of a (μ-oxo)bis(μ-carboxylato)diferric complex and hydrogen-bonded to the μ-oxo group.[3,10] It is not clear at this point whether the species described in this paper participates in the oxidative mechanisms of RNR R2 and MMO, since no oxygenated intermediates have thus far been observed for either protein. (The intermediates that have recently been found in the reaction of the diferrous RNR R2 with O_2 appear to be species that form subsequent to the cleavage of the O–O bond.) Nevertheless, the high likelihood that both iron centers in diferrous R2 have available coordination sites[20,56] and the possible homology between the diiron binding domain of RNR R2 and that proposed for MMO[57] make a μ-1,2-peroxide an important candidate to consider for the putative oxygenated intermediates of these enzymes.

The dioxygen adducts described in this paper exhibit significant differences in stability and reactivity. The adduct generated with the *N*-Et-HPTB ligand appears indefinitely stable at −60 °C in CH_2Cl_2 but decomposes upon warming. The addition of polar aprotic solvents extends its lifetime at higher temperatures and allows it to persist for 30 min even at ambient temperature. This adduct appears rather unreactive toward substrates. In contrast, the HPTP adduct requires the presence of polar aprotic solvents to be observed even at −80 °C and is capable of oxidizing 2,4-di-*tert*-butyphenol and Ph_3P. The enhanced electrophilicity of the bound dioxygen in the presence of pyridine ligands relative to benzimidazole ligands may arise from differences between the ligands in terms of basicity and steric bulk; however, further work is needed to clarify this question. Pyridine ligands have also been found to be more effective than benzimidazoles in the aromatic hydroxylation chemistry effected by dicopper complexes modeling tyrosinase activity[58] and in alkane functionalization reactions catalyzed by mononuclear ferric complexes in concert with *tert*-butyl hydroperoxide.[59]

Our present results demonstrate that the $3/O_2$ adduct can oxidize phenols. Thus, a (μ-peroxo)diiron(III) species is a plausible intermediate in the mechanism of tyrosyl radical formation in ribonucleotide reductase.[11] However, the dioxygen adducts we have generated do not react with the more difficult hydrocarbon substrates oxidized by methane monooxygenase. Thus, if a (μ-peroxo)diiron(III) species were involved in the latter mechanism, some further activation step would appear to be necessary to elicit oxygenation chemistry. The (η^2-peroxo)iron(III) porphyrin moiety has been proposed as an intermediate in the mechanism of cytochrome P-450, but has similarly turned out to be rather unreactive in model studies.[60] It has been suggested that O–O bond heterolysis may be facilitated by a Lewis acid. In model chemistry, acylation of the η^2-peroxide has been found to be effective in eliciting O–O bond cleavage.[59,61] For cytochrome $P\text{-}450_{cam}$, recent site-directed mutagenesis experiments have implicated Thr252 as a crucial player in the lysis of the O–O bond of the proposed peroxide intermediate.[62] Efforts are ongoing to uncover similar strategies for enhancing the oxidative power of these nonheme-iron dioxygen adducts.

Acknowledgment. This work was supported by the National Institutes of Health through Grant GM-38767 (L.Q.) and a predoctoral traineeship for B.A.B. (GM-08277). We acknowledge the valuable assistance of Dr. Yan Zang and Mr. Zhigang Wang in carrying out the NMR experiments.

Supplementary Material Available: Tables of atomic coordinates, thermal parameters, and bond lengths and angles for $[Fe_2(N\text{-Et-HPTB})(OBz)](BF_4)_2$ (33 pages). Ordering information is given on any current masthead page.

(53) Paul, P. P.; Tyeklár, Z.; Jacobson, R. R.; Karlin, K. D. *J. Am. Chem. Soc.* **1991**, *113*, 5322–5332.
(54) Goodson, P. A.; Oki, A. R.; Glerup, J.; Hodgson, D. J. *J. Am. Chem. Soc.* **1990**, *112*, 6248–6254.
(55) (a) Chiou, Y.-M.; Que, L., Jr. *J. Am. Chem. Soc.* **1992**, *114*, 7567–7568. (b) Zang, Y.; Que, L., Jr. Unpublished observations.
(56) McCormick, J. M.; Reem, R. C.; Foroughi, J.; Solomon, E. I.; Bollinger, J. M.; Stubbe, J.; Jensen, G. M.; Stephens, P. J. *New J. Chem.* **1991**, *15*, 439–444.
(57) Nordlund, P.; Dalton, H.; Eklund, H. *FEBS Lett.* **1992**, *307*, 257–262.
(58) (a) Tyeklár, Z.; Karlin, K. D. *Acc. Chem. Res.* **1989**, *22*, 241–248. (b) Sorrell, T. N.; Garrity, M. L. *Inorg. Chem.* **1991**, *30*, 210–215.
(59) Leising, R. A.; Norman, R. E.; Que, L., Jr. *Inorg. Chem.* **1990**, *29*, 2553–2555.
(60) Burstyn, J. N. Ph.D. Thesis, UCLA, 1986.
(61) Groves, J. T.; Watanabe, Y.; McMurry, T. J. *J. Am. Chem. Soc.* **1983**, *105*, 4489–4490.
(62) (a) Imai, M.; Shimada, H.; Watanabe, Y.; Matsushima-Hibiya, Y.; Makino, R.; Koga, H.; Horiuchi, T.; Ishimura, Y. *Proc. Natl. Acad. Sci. U.S.A.* **1989**, *86*, 7823–7827. (b) Martinis, S. A.; Atkins, W. M.; Stayton, P. S.; Sligar, S. G. *J. Am. Chem. Soc.* **1989**, *111*, 9252–9253.